Analytical Methods

Accepted Manuscript

This article can be cited before page numbers have been issued, to do this please use: T. Goldberg, R. Haseneder and A. S. Braeuer, *Anal. Methods*, 2026, DOI: 10.1039/D6AY00600K.

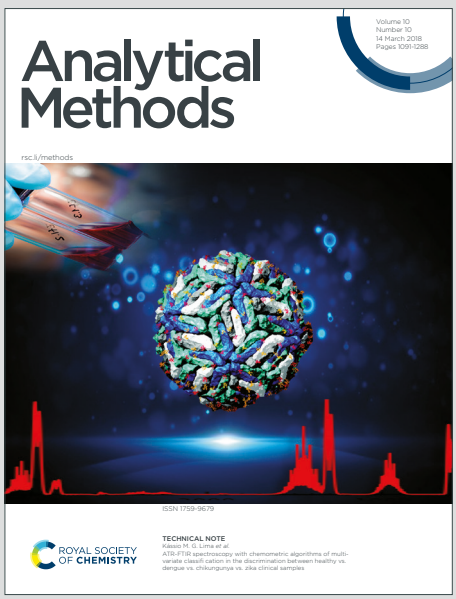

ROYAL SOCIETY OF CHEMISTRY

rsc.li/methods

View Article Online
DOI: 10.1039/D6AY00600K

Raman composition analysis of electrolyte solvent mixtures from industrial lithium-ion battery (LIB) recycling

Tom Goldberg, Roland Haseneder, Andreas S. Braeuer*

Institute of Thermal-, Environmental- and Resources' Process Engineering,

Technische Universität Bergakademie Freiberg, Leipziger Str. 28, 09599 Freiberg, Germany

*Corresponding author: Andreas.Braeuer@tun.tu-freiberg.de

Keywords

Solvent refinement, Battery recycling, Raman spectroscopy, Electrolyte solvents, Composition analysis, SERDS, CLS, PLS

Abstract

We report a Raman spectroscopy method for the quantitative analysis of electrolyte solvent mixtures from industrial lithium-ion battery recycling processes. Compositions of the electrolyte solvent mixtures were evaluated using classical least squares (CLS) and partial least squares (PLS) regression, which were compared in terms of accuracy, robustness, and applicability. CLS regression outperformed PLS, achieving mean absolute deviations of 0.006%mol/mol for binary and 0.018%mol/mol for quinary mixtures. Importantly, the approach includes a straightforward strategy to assess low-abundance compounds, providing an illustrative method to determine whether trace compounds should be included or excluded in the quantitative model.

View Article Online
DOI: 10.1039/D6AY00600K

Having developed the method with 310 synthesized mixtures of common organic carbonates spanning binary to quinary systems, we successfully quantified real condensate samples from two different battery recycling shredders with markedly different fluorescence backgrounds. Shifted Excitation Raman Difference Spectroscopy (SERDS) in the near infrared spectral region enabled reliable extraction of Raman signals and subsequent robust mixture quantification, by also effectively suppressing etaloning.

Introduction

Concerning the EU regulation on batteries and waste batteries, spent Lithium-ion batteries (LIBs) must be recycled at a minimum rate of 70 wt.% by the end of 2030[1]. Current LIB recycling mainly targets solid cathode or anode materials[2,3] and lithium recovery[4], while the liquid electrolyte – accounting for approximately 10-15 % of the cell mass[5] – receives little attention and may represent a critical lever for achieving future recycling targets. Moreover, the organic carbonates present in LIB electrolytes are increasingly recognized as green solvents and valuable platform chemicals for sustainable chemical production in Europe.

During some LIB shredding process or in subsequent black mass drying, the electrolyte solvents are removed as vapor under vacuum and subsequently condensed in a cold trap. Real-time composition analysis of these liquid electrolyte solvent mixtures not only enables the energy and time efficient control of the black mass drying process itself, but also – in order to meet future recycling targets – may contribute to the control of a prospective fractionation of the mixture into its pure compounds, e.g., via rectification. We therefore report the development of Raman

View Article Online
DOI: 10.1039/D6AY00600K

spectroscopy for rapid composition analysis of electrolyte solvent mixtures obtained from LIB recycling. We chose Raman spectroscopy, as it enables the detection of highly resolved spectra over wide ranges of Raman shifts with non-complex equipment[6,7], which is prerequisite for the deconstruction of mixture spectra into the mixture constituent spectra, especially if the constituents are chemically similar like LIB electrolyte solvents. Short wavelength infrared (SWIR) absorption spectroscopy on the contrary, provides poorly resolved spectra, which makes the spectral deconstruction challenging.[8] Fourier transformed infrared absorption spectroscopy (FTIR) enables the detection of highly resolved spectra, but only when using special and highly sensitive optical access ports[7], which will cause challenges when the measurement technique is to be transferred to its industrial application. And, especially for the spectral range of wavenumbers smaller than 700 cm^{-1} thermal detectors are utilized[9], which require a cooling of at least the sample mixture.

Due to differences between LIB types, generations and manufacturers, electrolyte solvent mixtures vary in composition, which results in more complex mixtures in the recycling process. Nevertheless, five organic carbonates typically constitute the main solvent compounds[10–13]: dimethyl carbonate (DMC), ethyl methyl carbonate (EMC) and diethyl carbonate (DEC) as lower boiling compounds as well as ethylene carbonate (EC) and propylene carbonate (PC) as higher boiling compounds. Wolke et al.[14] analyzed electrolyte solvent mixtures from spent LIBs in detail using GC-MS and GC-FID. Their study covers a broad range of additives and trace-level impurities from aging or processing. In contrast, our work does not aim at trace analysis but focuses on the rapid quantification of the main compounds to enable fast decision-making and improved process control. In particular, Raman spectroscopy can prevent sampling, which is especially advantageous

View Article Online
DOI: 10.1039/D6AY00600K

given the potential presence of toxic residues or degradation products in the electrolyte mixtures from LIB recycling.[11]

Accurate composition analysis of liquid mixtures using Raman spectroscopy relies on the availability of meaningful Raman spectra. Laser-induced fluorescence of even trace amounts of impurities can heavily interfere with the desired Raman spectrum and render a reliable evaluation. Techniques for fluorescence suppression/rejection are therefore essential and can be broadly divided into experimental and computational approaches.[15] Computational methods allow the mathematical removal of fluorescence backgrounds from recorded spectra without additional experimental effort. They are applicable whenever the Raman spectrum is still recognizable next to the fluorescence interference. The variety of specific computational methods is comprehensively reviewed in the literature[15,16], and generally exploits the difference in curvature or frequency between the broad fluorescence background and the narrow Raman peaks. Machine-learning (ML) or deep-learning (DL) based approaches are increasingly being investigated for fluorescence correction in Raman spectroscopy. These methods can learn complex spectral relationships and fluorescence characteristics directly from experimental or synthetically augmented training data and may enable highly efficient automated spectral processing.[17] This is particularly advantageous for compound identification tasks. However, for fluorescence-dominated spectra computational processing may unintentionally distort Raman spectral features relevant for quantitative analysis, including relative peak intensities and peak shapes. This becomes particularly critical for complex multi-compound mixtures with overlapping Raman bands, where even small spectral deviations can compromise reliable composition analysis. Experimentally, larger excitation wavelength can

View Article Online
DOI: 10.1039/D6AY00600K

reduce the fluorescence background, albeit at the cost of lower Raman signal intensity.[16,18] Based on Kasha's rule[19], fluorescence emissions remain largely insensitive to small variations of the excitation wavelength, whereas Raman peaks spectrally shift accordingly. This behavior is exploited in experimental techniques such as Shifted Excitation Raman Difference Spectroscopy (SERDS). In SERDS, spectra are recorded at two slightly shifted excitation wavelengths and then subtracted, which removes the quasi-unchanged fluorescence background, while the Raman signal remains as a shifted difference.[20] The generation of clean Raman spectra from highly fluorescent samples using SERDS has been illustratively reported elsewhere.[21,22] In addition to fluorescence, Sheridan et al.[23] demonstrated that optical etaloning – an interference effect in detectors which often appears in the near infrared spectral region and which is often challenging to remove from the signal of interest – can be suppressed using SERDS.

A number of methods for composition evaluation from Raman spectra exist in the literature.[24–32] However, present studies are mostly limited to synthetic mixtures with only a few compounds, or to the identification of some target compounds in more complex systems. Two general approaches are commonly employed and are also compared in this study: chemometric and physics-based regression models. Chemometric models, such as partial least squares (PLS) regression, are particularly well suited for high-dimensional and highly collinear spectral data.[33] AI-based methods for quantitative composition evaluation, which can be considered as an extension of classical chemometric approaches, typically require extremely large training datasets and were excluded from this study owing to limitations in both time and perspective industrial feasibility. Data augmentation methods may partially compensate for limited experimental datasets; however,

View Article Online
DOI: 10.1039/D6AY00600K

synthetically generated spectra are commonly based on predefined assumptions regarding spectral variations, which may introduce artificial correlations into the training data. This can limit the generalizability and robustness of the resulting models, which is particularly critical for real recovery streams from battery recycling with variable compositions and possible impurities. The conceptually simplest physics-based model is classical least squares (CLS) regression, which can provide better interpretability compared to chemometric models, but requires the spectra of the pure compounds included in the mixture.[28] To overcome this limitation, more advanced physics-based approaches, including indirect hard modeling (IHM)[34] and other peak decomposition methods[28], have been developed, allowing analysis of mixtures without complete reference spectra and accounting for phenomena such as peak shifts. However, in multi-compound mixtures with multiple overlapping peaks, the number of model parameters may readily exceed several hundred[32], potentially making parameter identifiability extremely challenging or unfeasible.

Building on insights from the literature, this study aims to contribute to two aspects: specifically, it focuses on the rapid quantification of electrolyte solvent mixtures from lithium-ion battery recycling, while generally, the study aims to advance Raman spectroscopy for the analysis of multi-compound mixtures. The article is organized as follows. First, composition evaluation strategies are developed based on numerous synthesized non-fluorescent mixtures ranging from binary to higher-order systems and compared in terms of accuracy and robustness. The models are then applied to real samples obtained from two different LIB recycling shredders. Based on this, the study also explores the use of SERDS to address specific spectral interferences in real samples, providing a framework for robust analysis of complex electrolyte solvent mixtures.

View Article Online
DOI: 10.1039/D6AY00600K

Methods

Materials and sample preparation

DMC (CAS: 616-38-6), DEC (CAS: 105-58-8), EC (CAS: 96-49-1), and PC (CAS: 108-32-7) were purchased from Carl Roth (synthesis grade, certified purity >99.9 %), whereas EMC (CAS: 623-53-0) was only available with a purity of 98.3 %. Real condensate samples were provided by the Institute of Mechanical Process Engineering and Mineral Processing (MVTAT) at TU Bergakademie Freiberg (TUBAF), which operates a pilot-scale battery shredder processing various end-of-life batteries, particularly from the automotive sector. Additional samples were provided by BASF SE, operator of one of the largest lithium-ion battery recycling facilities in Europe in Schwarzheide, Germany. In the following, condensate samples originating from these shredders are referred to as pilot shredder (MVTAT/TUBAF) and industrial shredder (BASF SE). Additionally performed gas chromatography-mass spectrometry (GC-MS, Agilent 7890A, 5975C mass spectrometer, HP5-MS 30 m column), revealed some proportions of tert-butylbenzene (TBB, CAS: 98-06-6) and tert-pentylbenzene (TPB, CAS: 2049-95-8) in the condensate samples, which were purchased from Fisher Scientific GmbH with purities of 99 % and 97 %, respectively.

Synthetic mixtures with a total mass of approximately 3 g were prepared gravimetrically using an analytical balance (ABJ 320-4NM, KERN & SOHN GmbH, readability: 0.0001 g). In order to cover all possible and potentially unpredictable compositions of electrolyte solvent recovery streams, about 230 different binary mixtures were prepared, covering all combinations of DMC, EMC, DEC, EC, and PC across the full composition range (0-1 mol/mol) for calibration. This broad

View Article Online
DOI: 10.1039/D6AY00600K

calibration matrix was also intentionally designed to evaluate the capability of the models to describe binary compound interactions across the complete composition range. In contrast, TBB as LIB electrolyte additive was calibrated primarily at lower mole fractions; TPB was excluded due to its lower purity and limited availability at high cost, particularly since GC-MS analysis indicated only trace amounts of TPB in the real condensate samples, which were within the uncertainty range of our Raman method. Additionally, about 80 higher-order (ternary to quinary) mixtures of the organic carbonates were prepared to access the transferability from binary to multi-compound systems providing a more realistic approximation of real condensate mixtures from LIB shredders.

Experimental setup

All measurements were conducted at 298.15 K in an air-conditioned laboratory under ambient pressure. The spectra of the pure compounds were measured using a large-volume cuvette (Type 700-OG 22,500 µL with glass lid, Hellma GmbH). In order to prevent evaporation, all mixture samples were prepared and measured directly in sealed vials. To assess measurement repeatability and reproducibility selected samples were measured several times as well as on different days and repositioned between measurements. In order to prevent crystallization, samples rich in EC were heated to 50 °C before measurement. Potential peak shifts or other changes in composition quantification due to temperature differences were ruled out by testing. The Raman setup is schematically illustrated in Figure 1.

View Article Online
DOI: 10.1039/D6AY00600K

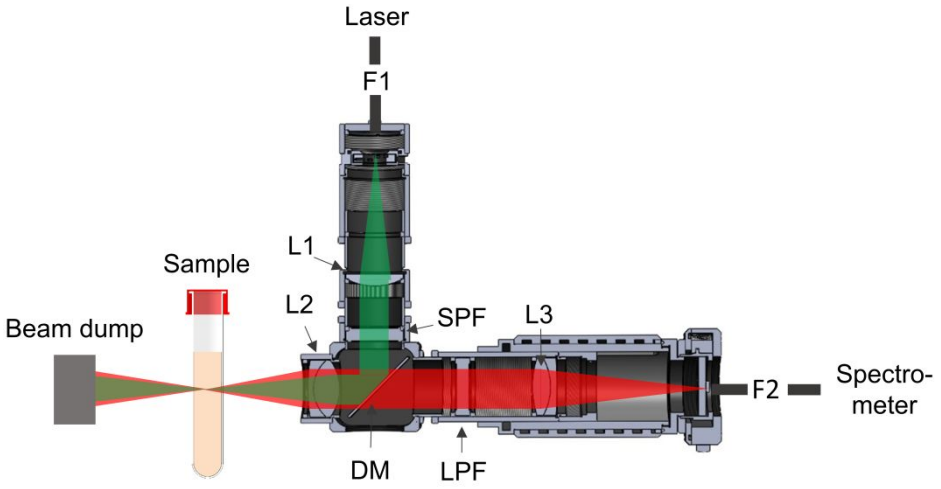

Figure 1: Schematic illustration of the Raman probe (F-Fiber, L-Lens, SPF-Short-pass filter, LPF-Long-pass filter, DM-Dichroic mirror). Adapted from Willger & Braeuer[35].

The samples were excited using an amplified tunable diode laser system (TEC420-0785-3000, Sacher Lasertechnik GmbH, Germany) with a tunable wavelength range between 770-790 nm. The laser linewidth was specified to be < 0.5 MHz over 50 ms and < 5 MHz over 20 s, which is well below the spectral resolution of the spectrometer. For conventional Raman spectroscopy, the excitation wavelength was set to 784.0 nm. For SERDS measurements, the samples remained in position, and a second spectrum was directly acquired after shifting the excitation wavelength to 784.6 nm using the integrated DC motor via motor control software. The laser power at the sample position was measured to be (765 ± 4) mW and showed no systematic dependence on the excitation wavelength (784.0 nm vs. 784.6 nm) within the measurement uncertainty; small step-like variations in power were observed upon wavelength switching, attributed to the motor-controlled tuning mechanism. Lenses L1 (LA1422-B-ML, Thorlabs, $f = 40$ mm) and L2 (AC254-030-B, Thorlabs, $f = 30$ mm) image the fiber-optic output of glass fiber F1 (M25L, Thorlabs, Ø200 µm) into the

View Article Online
DOI: 10.1039/D6AY00600K

measurement volume. A short-pass filter SPF (Thorlabs FESH0800) removes broadband background probably generated in the excitation fiber. Lenses L2 and L3 ($f = 40$ mm) then image the elastically and inelastically scattered light from the sample into the detection fiber F2 (VIS/NIR Ocean Optics, Ø600 µm), where the red-shifted light can pass the dichroic mirror DM (DMLP805R, Thorlabs) and an additional long-pass filter LPF (RazorEdge LP808 RE, Semrock). The spectra are recorded using a spectrometer (QE Pro, Ocean Optics, 50 µm slit). Additionally, a similar Raman setup with an excitation wavelength of 532 nm was tested, which is described in detail elsewhere.[35]

Spectra acquisition and processing

For each mixture, a total of 20 spectra were recorded with integration times of 1000 ms for conventional Raman measurements and – in order to avoid spectrometer saturation – 30 ms for highly fluorescent samples measured with SERDS. The spectra were then averaged arithmetically and area-normalized; additional processing steps required for SERDS are described in detail in the results section. In order to preserve maximum spectral information for mixture quantification, the complete fingerprint range (400 – 1600 cm^{-1}) of the obtained spectra was evaluated using the regression models.

PLS regression model

In partial least-squares (PLS) regression, both the spectral data matrix and the composition matrix are directly projected onto a reduced set of latent variables. In this study, PLS was applied solely

View Article Online
DOI: 10.1039/D6AY00600K

for the quantitative analysis of synthetic mixtures. However, prior to regression, the background signal of each mixture spectrum was subtracted by iteratively estimating the broad baseline with a polynomial of fixed fourth-degree, following the approach of Gan et al.[36] From testing, this proved more robust than using an asymmetric least squares (ALS) algorithm[37] for background fitting and subtraction. Model training was then performed on synthetic mixtures using the plsregress function in MATLAB 2023b. The optimal number of latent variables was determined using 10-fold cross-validation by minimizing the mean squared error.

CLS regression model

The spectral features of the pure compounds are preserved in the mixture spectra in terms of peak positions and intensities [38], which forms the basis of the physics-based classical least-squares (CLS) regression model. Under the assumption of linear additivity of Raman signals, each modelled mixture spectrum

$$\hat{S}_{mix}(\nu) = \sum_{i=1}^{N} w_i S_i(\nu + \Delta\nu_i) + b\, B(\nu + \Delta\nu_B) + \sum_{k=0}^{4} p_k \nu^k \quad (1)$$

can ideally be expressed as a linear combination of the pure compound spectra S_i (linear unmixing) at Raman shift ν with weighting factors w_i, where i denotes the mixture compound. In contrast to the PLS model, the background was simultaneously modelled using a measured background spectrum B (glass signal of the air-filled cuvette) scaled by fitting parameter b, and – in order to describe the broad fluorescence background – a fourth-degree polynomial function with fitting

View Article Online
DOI: 10.1039/D6AY00600K

parameters p_k. Small global shifts of the pure compound spectra and the measured background spectrum, which may arise from minor instrumental variations, were accounted for by the parameters $\Delta\nu_i$ and $\Delta\nu_B$, respectively.

All fitting parameters

$$\{w_i,b,p_k,\Delta\nu_i,\Delta\nu_B\} = \arg\min \sum_\nu r(\nu)^2, \quad (2)$$

up to 21 parameters for a mixture containing 7 compounds, were identified by minimizing the sum of squared residuals

$$r(\nu) = S_{mix}(\nu) - \hat{S}_{mix}(\nu) \quad (3)$$

between the measured $S_{mix}(\nu)$ and modelled $\hat{S}_{mix}(\nu)$ mixture spectrum.

From this fitting procedure, a set of weights w_i was obtained for each mixture spectrum, which – owing to area normalization of the spectra – directly correspond to the Raman signal intensities of the compounds in the mixture. From theoretical considerations, the ratio of Raman signal intensities is direct proportional to the ratio of the corresponding mole fractions of two compounds x_i and x_j with the binary calibration constant K_{ij}[38]. However, these binary calibration constants are not independent. For any third compound l, they must satisfy $K_{ij} = \left(\frac{K_{lj}}{K_{li}}\right)_{l\neq i\neq j}$. Therefore, in order to simplify the formulation for multi-compound mixtures, the binary calibration constants are expressed in terms of ratios of compound-specific constants k_i:

View Article Online
DOI: 10.1039/D6AY00600K

$$\frac{w_i}{w_j} = \frac{k_j}{k_i}\ \frac{x_i}{x_j} \tag{4}$$

Taking the natural logarithm of both sides

$$\ln k_i - \ \ln k_j = \ln\left(\frac{x_i}{x_j}\right)\ - \ln\left(\frac{w_i}{w_j}\right) \tag{5}$$

yields the linearized equation or in matrix form

$$\overbrace{\begin{pmatrix} 1 & -1 & 0 & \dots & 0 \\ 1 & 0 & -1 & \dots & 0 \\ \vdots & \vdots & \vdots & \ddots & \vdots \\ 0 & \cdots & \cdots & 1 & -1 \end{pmatrix}}^{\mathrm{A}} \overbrace{\begin{pmatrix} \ln k_1 \\ \ln k_2 \\ \vdots \\ \ln k_n \end{pmatrix}}^{\vec{y}} = \overbrace{\begin{pmatrix} \ln(x_1/x_2) - \ln(w_1/w_2) \\ \ln(x_1/x_3) - \ln(w_1/w_3) \\ \vdots \\ \ln(x_{n-1}/x_n) - \ln(w_{n-1}/w_n) \end{pmatrix}}^{\vec{b}} \tag{6}$$

considering n compounds in the mixture. Therefore, coefficient matrix $\underline{A}$ is well-conditioned, containing only values +1, −1, and 0, ensuring numerical stability. Since more binary calibration mixtures were prepared than compounds involved, the system of equations is overdetermined and solved using the direct least-squares solver in MATLAB 2023b. This formally yields n constants k_i , one for each compound; however, mathematically only the ratios k_i/k_j are defined, so – in order to provide a common reference – the constants were normalized to a geometric mean of unity.

View Article Online
DOI: 10.1039/D6AY00600K

Results and discussion

Measurement and evaluation strategy

Figure 2 presents an example synthetic mixture and representative condensate samples obtained from the two lithium-ion battery shredders described above, together with their raw Raman spectra (area-normalized) recorded using the 532 nm and 784 nm as excitation wavelengths.

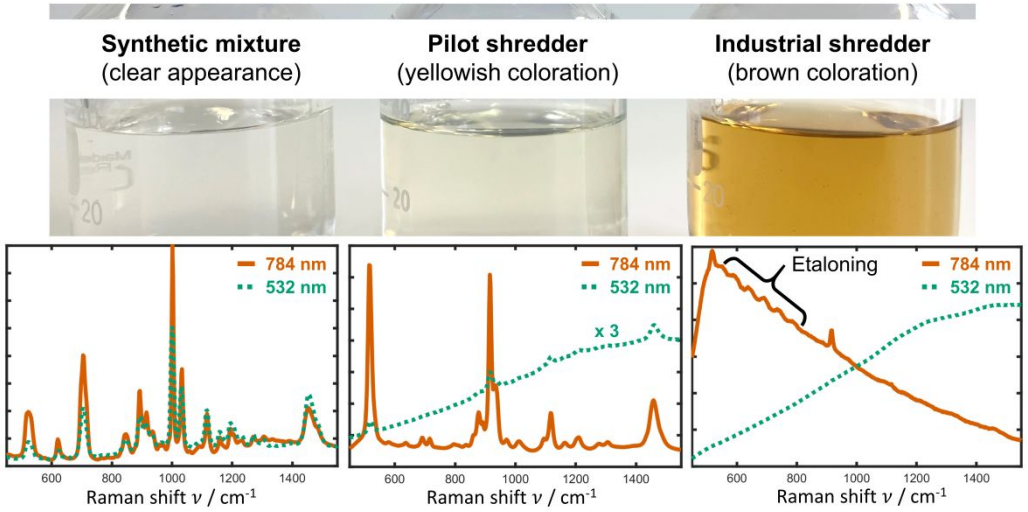

Figure 2: Visual appearance of a synthetic mixture and representative condensate samples from the two lithium-ion battery shredders along with their corresponding area-normalized raw Raman spectra excited with 532 nm and 784 nm.

The pure organic carbonates and their synthetic mixtures are clear and colorless, whereas the condensate samples from pilot shredder appear yellowish, likely due to partial thermal degradation of the organic carbonates. The condensate samples from industrial shredder exhibit a dark yellow to brown coloration, possibly originating from contamination by black mass components or other processing residues.

View Article Online
DOI: 10.1039/D6AY00600K

From this differing appearance, the synthetic mixtures show Raman spectra with only a marginal background, while the condensate samples from pilot and industrial shredder – when excited with 532 nm – exhibit strong fluorescence interferences that significantly overlap the Raman signal, preventing the reliable interpretation of Raman features. For the samples obtained from pilot shredder, the broadband fluorescence interferences can be largely reduced by using the longer excitation wavelength of 784 nm. In the case of the samples from industrial shredder, characteristic Raman bands (e.g., at 500 and 900 cm^{-1}) then become visible; however, even the NIR-excited Raman spectra remain fluorescence-dominated. In addition, etaloning effects appear in the region from 550 to 800 cm^{-1} (Figure 2), additionally interfering the Raman signals.

Based on this comparison, the subsequent measurement strategy was adopted: the 784 nm Raman setup was exclusively used to minimize fluorescence background already during acquisition. Therefore, conventional Raman spectroscopy was sufficient for the synthetic mixtures and condensate samples from pilot shredder, where the remaining background could be removed by subtraction in the PLS model or by polynomial fitting in the CLS model. In contrast, samples from industrial shredder were analyzed using SERDS to enable the experimental separation of the Raman signal from the strong fluorescence background along with etaloning.

In order to illustrate the characteristic Raman features of the individual compounds, Figure 3 shows the area-normalized experimental spectrum S_{mix} of an equimolar synthetic mixture at the top together with the spectra S_i of the underlaying pure compounds excited with 784 nm.

View Article Online
DOI: 10.1039/D6AY00600K

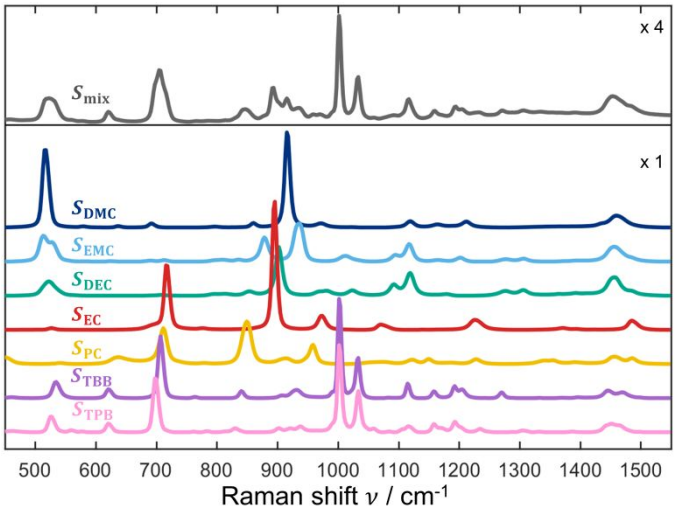

Figure 3: Area-normalized Raman spectrum of an equimolar synthetic mixture and the corresponding spectra of the pure compounds DMC, EMC, DEC, EC, PC, TBB, and TPB excited with 784 nm.

Due to the structural similarities of the different organic carbonate molecules, the pure compound spectra S_i show significant peak overlaps. The mixture spectrum demonstrates that the entire fingerprint region (400–1600%cm^{-1}) contains relevant features, justifying its full evaluation in the regression models to preserve maximum spectral information for mixture quantification. This also motivates the relatively large data sets for calibration/training and testing of the models for evaluating the composition of such multi-compound mixtures.

In the following sections, the development of composition evaluation methods is illustrated, beginning with simple synthetic mixtures, based on which the CLS and the PLS models are compared. Compositions of low-fluorescent samples (condensate from pilot shredder) and high-

View Article Online
DOI: 10.1039/D6AY00600K

fluorescent samples (condensate from industrial shredder) are then evaluated by adapting the methods.

Model development on synthetic mixtures

The PLS model was trained and applied straightforwardly using the MATLAB routine described above, whereas the physics-based CLS model provides additional interpretative capability, enabling detailed analysis of individual compound contributions; these results are presented below.

Initial weight assignment in CLS model

Figure 4 illustrates the reconstruction of an example quinary synthetic mixture spectrum (excluding TBB and TPB) according to equation 1. The measured spectrum (Figure 4 top left) is decomposed into the individual compound contributions $w_i S_i$, the weighted background bB, and a polynomial baseline $\sum_{k=0}^{4} p_k \nu^k$, with the residual r (equation 3) minimized between measured and modelled spectrum (Figure 4 bottom left gray).

View Article Online
DOI: 10.1039/D6AY00600K

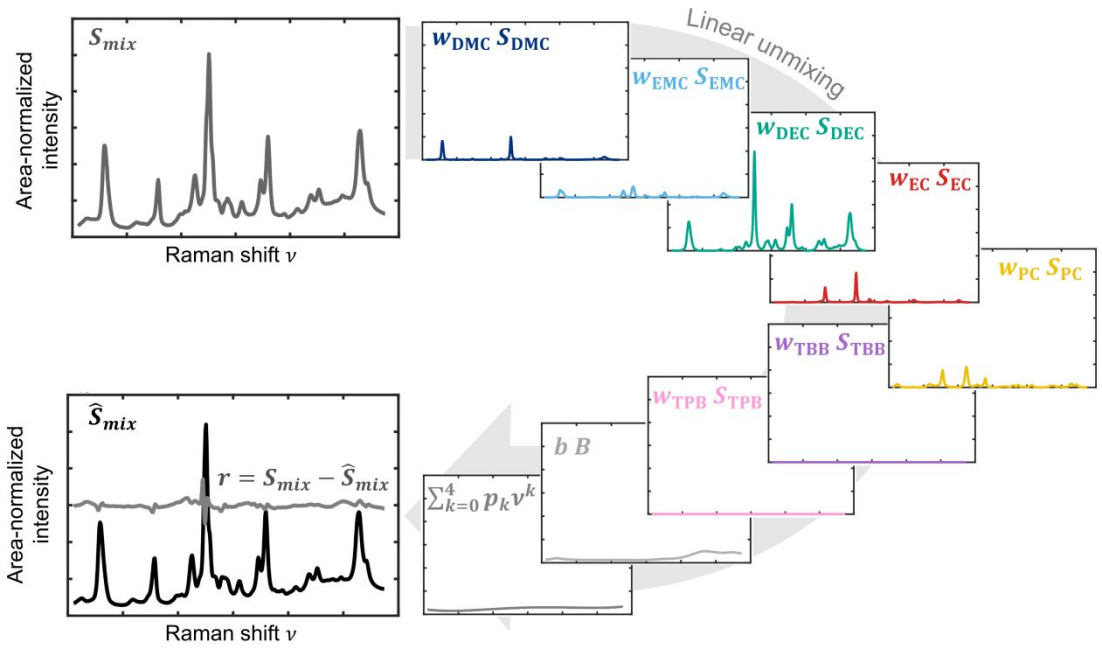

Figure 4: Linear unmixing (CLS model) of an example quinary synthetic mixture.

Based on the small residual r, the modelled spectrum closely matches the measured spectrum, indicating that the CLS model captures the contribution of each compound well. Notably, TBB and TPB were correctly assigned quasi-zero weights (weighted intensities w_i are quasi-zero), confirming that the model does not attribute signal to absent compounds. Vice versa, the residual spectrum also provides an important diagnostic tool: any systematic features or remaining spectral structure in the residual spectrum r would indicate the presence of unaccounted compounds. This feature is not available with the PLS approach and particularly valuable for future analyses of complex condensate samples as it ensures prompt recognition of possible electrolyte additives or processing residues.

View Article Online
DOI: 10.1039/D6AY00600K

Binary calibration of the CLS model

Following the spectrum reconstruction example, the CLS model was calibrated using all prepared binary mixtures with known composition, determining the weighting factors w_i for each compound pair. Figure 5 illustrates example spectral intensity data and their linear unmixing for binary DMC-DEC (left side) and DMC-PC (right side) mixtures with increasing DMC mole fractions, minimizing the deviation between the measured spectrum (gray line) and modelled spectrum (black line). In the upper left corner of each diagram the ratio of the fitted weighting factors w_i/w_j is shown together with the corresponding ratio of the prepared mole fractions x_i/x_j.

View Article Online
DOI: 10.1039/D6AY00600K

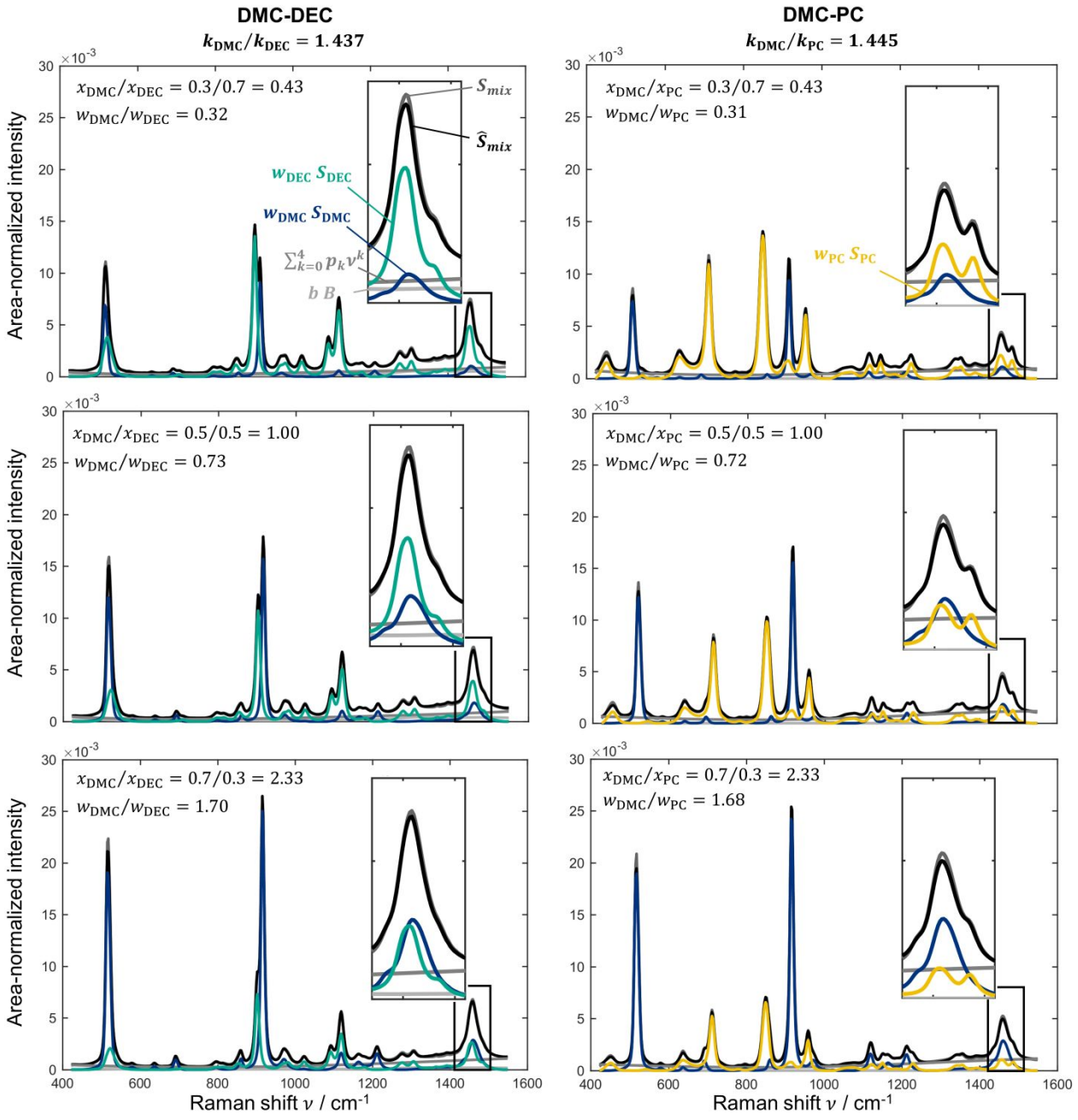

Figure 5: Linear unmixing of example spectra of binary mixtures DMC-DEC (left) and DMC-PC (right) with DMC mole fractions of 0.3, 0.5 and 0.7 mol mo1^{-1}.

The diagrams in Figure 5 (from top to bottom) illustrate the relative increase of the spectral area of DMC with increasing mole fraction, which is also expressed in the increasing ratio of the weighting

View Article Online
DOI: 10.1039/D6AY00600K

factors. Analogously, the weighting factor ratios w_i/w_j were determined for all binary calibration mixtures with known composition ratios x_i/x_j. The calibration constants were then calculated for all compounds at once by solving equation 5 or 6, respectively. When plotting the composition ratios x_i/x_j against the determined weighting factor ratios w_i/w_j, the data points for each binary system i/j fall on a straight line with slope k_i/k_j (Figure 5 top), confirming the assumed linear combination of intensity in accordance with equation 4. Figure 6 shows the resulting parity plots for each compound (see diagram label) in all binary mixtures (see symbols). As noted previously, calibration for TPB as electrolyte additive was omitted due to limited availability and purity, and because the mole fractions detected with GC-MS in the real samples were very low (< 0.003 mol mol^{-1}) and within the uncertainty of the Raman method. The dotted lines indicate the root mean squared error (RMSE) interval around the parity line for each compound. Error bars representing the reproducibility of the Raman measurements (0.002 mol mol^{-1}, see below for details) and uncertainties from mixture preparation, evaluated following the Guide to the expression of uncertainty in measurement (GUM) via propagation of the combined balance uncertainty ($u(m) \approx 0.0002$ g), are smaller than the marker size and therefore not visible.

View Article Online
DOI: 10.1039/D6AY00600K

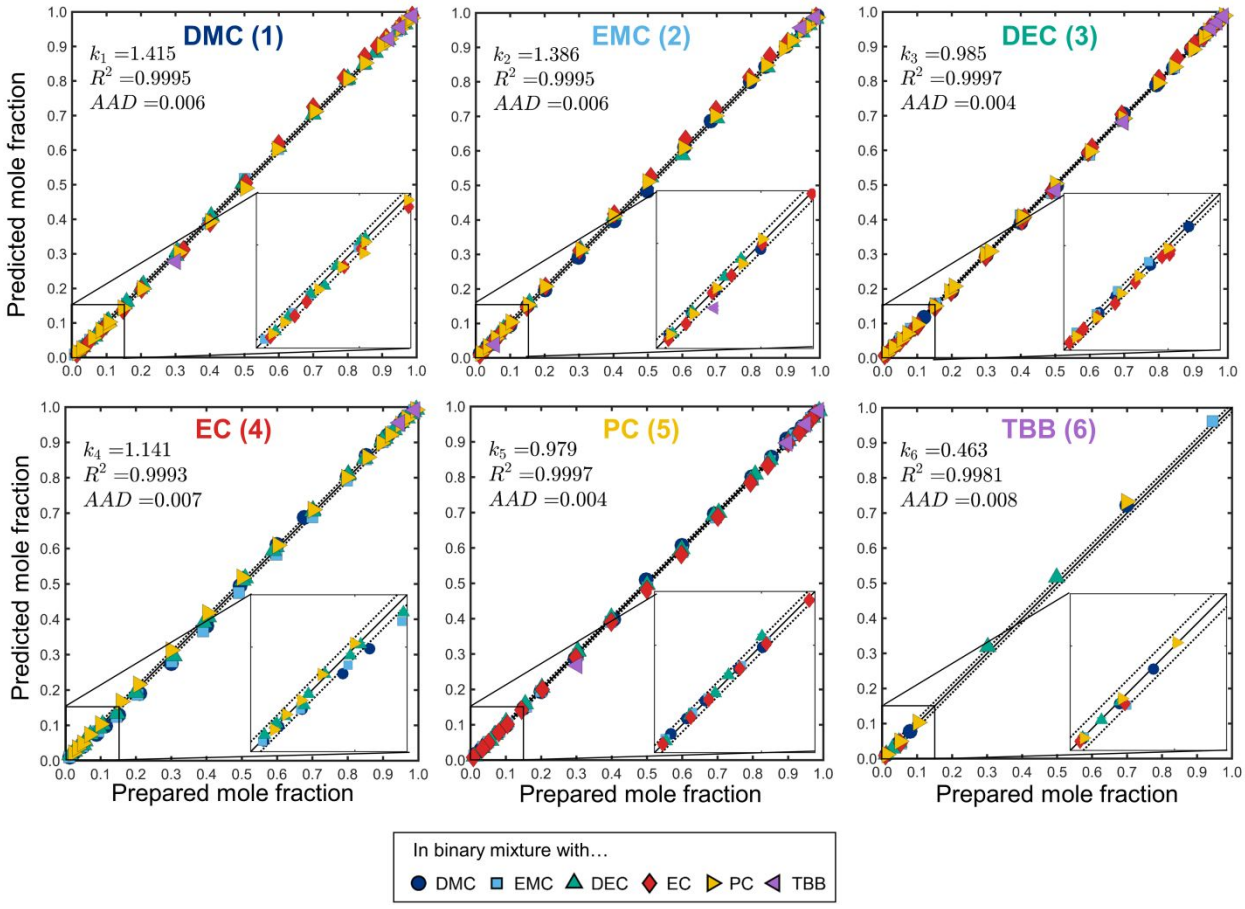

Figure 6: Fitting of calibration constants in CLS model: Parity plots comparing predicted vs. prepared mole fraction for each compound in binary mixtures. Dotted lines represent the RMSE interval around the parity line. Error bars are not visible because the uncertainties from Raman measurement reproducibility and mixture preparation are smaller than the marker size.

Based on the parity plots, the linear CLS model adequately describes the interactions between all investigated compounds across the full composition range from 0 to 1 mol/mol, which supports its applicability for the analysis of highly variable LIB electrolyte recovery streams. The majority of data points lie within the RMSE interval, indicating high precision of the model predictions. The mean absolute deviation (AAD) for all binary synthetic mixtures is 0.006 mol mol^{-1}, which is

View Article Online
DOI: 10.1039/D6AY00600K

mainly related to the goodness of fit of the regression model together with potential uncertainties from sample preparation or experimental variations. Such accuracy indicates that Raman spectroscopy in combination with CLS provides a reliable method for quantitative composition analysis of these binary mixtures, in principle. However, in contrast to calibration mixtures, where all included compounds are known, quantification becomes more challenging for unknown multi-compound mixtures, particularly when some compounds are present only in minor amounts. In such cases, careful parameter identification is required to avoid assigning weight to compounds that are not present, while at the same time ensuring that all truly present compounds are included in the model. Therefore, we propose a leave-one-compound-out algorithm as an intermediate step for multi-compound analysis of unknown mixtures, which is described in detail in the following subsection.

Weight refinement for unknown mixtures including minor species

As described in the methods section, the weights w_i in the CLS model were determined by minimizing the sum of squared residuals between the measured and modelled spectrum. Consequently, the contribution of each compound to the minimization can be quantified by comparing the residue minimized when considering all compounds and the residue $r_{(-i)}$ when considering all compounds except one. We therefore quantify the contribution of compound i to the minimization by the contribution index

$$\Delta R_i = \sum_\nu \big(r_{(-i)}(\nu) - r(\nu)\big), \tag{7}$$

View Article Online
DOI: 10.1039/D6AY00600K

which sums up the residue difference along the spectral axis. This index was computed for every compound i across all synthetic mixtures, ranging from binary to quinary compositions, regardless of whether the compound was present in the mixture (Figure 7 green dots) or not (Figure 7 gray circles). From the CLS model in equation 5 and for those compounds contained in the mixture, the resulting ΔR_i values are expected to be proportional to the corresponding weighting factors w_i. This relationship is illustrated for DEC in Figure 7, but the same analysis was performed for all other compounds accordingly.

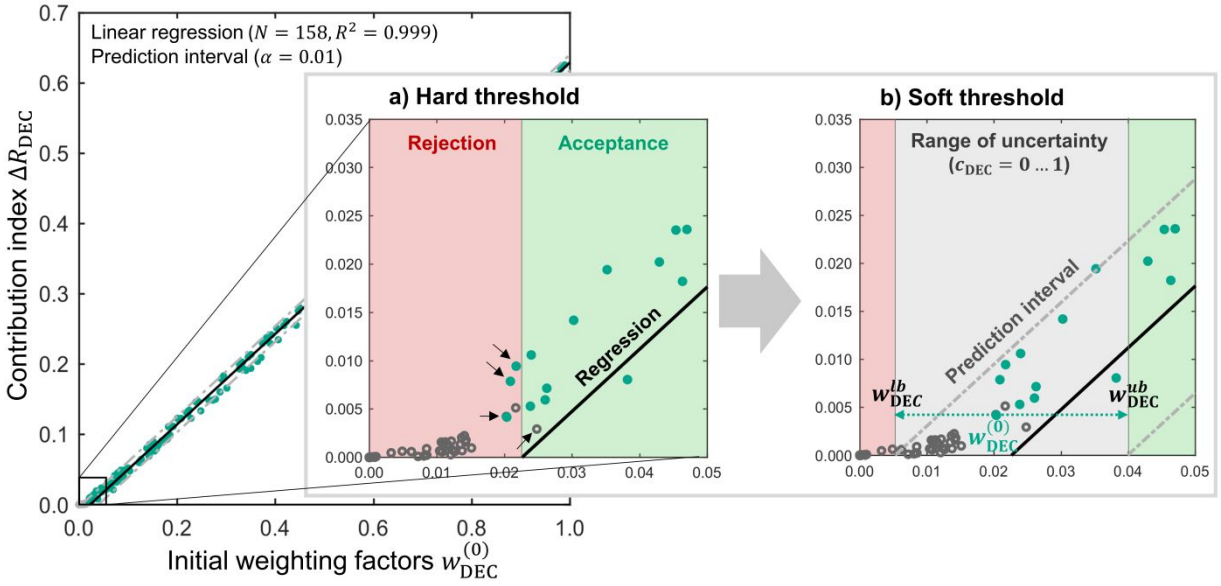

Figure 7: Linear relationship between initial DEC weighting factors and contribution index (green dots) for a range of multi-compound (binary to quinary) mixtures. Gray circles indicate mixtures in which DEC was assigned a non-zero weight despite being absent. Illustration of the proposed a) hard threshold and b) soft threshold.

View Article Online
DOI: 10.1039/D6AY00600K

Since a compound with zero weight should have no effect on the residual, the linear regression should ideally pass through the origin of the diagram. However, in practice, the regression exhibits a small positive root – weight at zero contribution index (see insets in Figure 7) – for all compounds, due to limitations in parameter identifiability and measurement noise. Using the root of this regression as a hard evaluation threshold (Figure 7a) may have negative consequences for the composition quantification of unknown mixtures. This is illustrated in Figure 7a by the data points highlighted by arrows. The three green discs represent mixtures that in fact contain DEC but whose weighting factor is evaluated smaller than the root of the regression $w_{\mathrm{DEC}} < 0.02$. They will erroneously be evaluated as mixtures not containing DEC. The gray highlighted circle represents the opposite, where some DEC will be assigned to a mixture that in fact is free of DEC. In order to decrease the risk of erroneously quantification of minor compounds, we follow the concept illustrated in Figure 7b. Considering a 10 % significance level, the grayly highlighted range between the two roots (w_i^{lb} and w_i^{ub} in Figure 7b) of the prediction interval defines a soft threshold range of weights, within which the effect of including the compound is ambiguous. If weights fall within this range CLS regression is performed by assuming all compounds are present in the mixture yielding the initial weights $w_i^{(0)}$. The acceptance factor c_i

$$c_i = \frac{w_i^{(0)} - w_i^{lb}}{w_i^{lb} - w_i^{ub}}, \qquad w_i^{lb} \le w_i^{(0)} \le w_i^{ub} \tag{8}$$

is then computed for each compound i and the new weight

View Article Online
DOI: 10.1039/D6AY00600K

$$w_i = c_i w_i^{(0)} + (1 - c_i) w_i^{(1)} \quad (9)$$

is updated.

Comparison of PLS and CLS with synthetic mixtures

With the CLS model calibrated and the soft threshold ranges for every compound determined, the compositions of multi-compound (binary to quinary) synthetic mixtures were evaluated using both the CLS and PLS models. Figure 8 shows the corresponding parity plots for composition predictions obtained with the two approaches. The dotted lines indicate the RMSE interval around the parity line for each mixture order. Error bars representing the reproducibility of the Raman measurements and the uncertainty associated with mixture preparation are smaller than the marker size and therefore not visible.

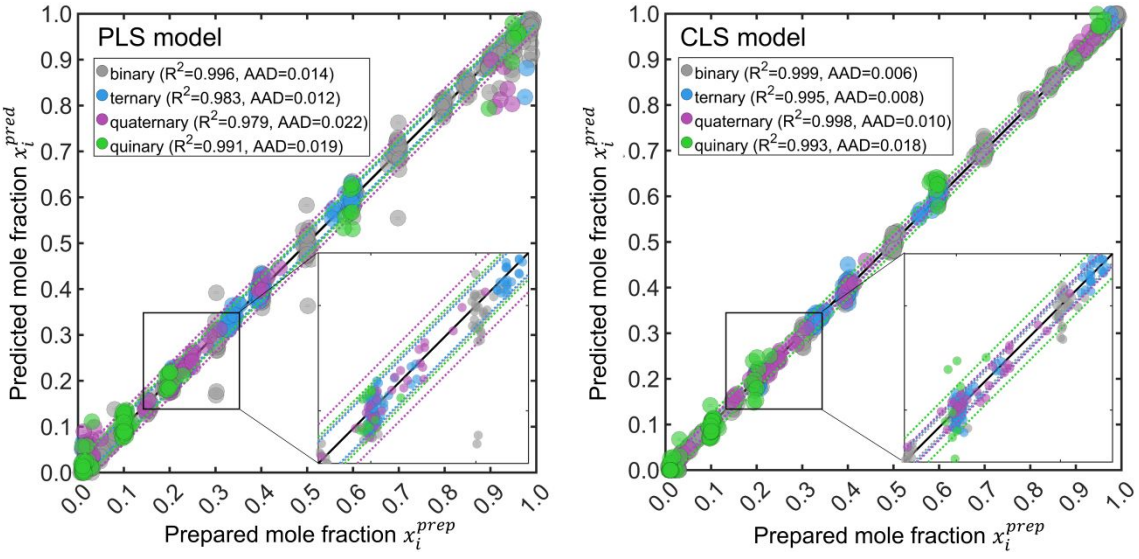

Figure 8: Parity plot of PLS model (left) and CLS model (right) trained or, respectively, calibrated with binary mixtures and applied on higher-order mixtures. Dotted lines represent the RMSE

View Article Online
DOI: 10.1039/D6AY00600K

interval around the parity line for each mixture order. Error bars are not visible because the uncertainties from Raman measurement reproducibility and mixture preparation are smaller than the marker size.

The physics-based CLS regression model enables composition quantification with higher accuracy and particularly higher precision compared to the PLS model. For binary mixtures composed solely of organic carbonates, the mean absolute deviation of the PLS predictions is also below 0.01 mol mol^{-1}, suggesting that PLS could also be suitable for prospective online process monitoring. However, larger discrepancies appear in mixtures containing TBB, especially at intermediate compositions, where only a few training mixtures were used. Overall, the PLS model exhibits decreasing accuracy and precision at both low and high mole fractions (due to the summation constraint of mole fractions to 1), indicated by broader RMSE intervals and more pronounced deviations from the parity line. In contrast, the CLS approach maintains robust performance across the full composition range. The average deviations of the CLS model slightly increase when applied to higher-order synthetic mixtures, but are still below 0.02 mol mol^{-1} for quinary mixtures. Additional sources of error may arise from sample preparation, particularly when handling multiple compounds, as well as from significant spectral overlaps, which can reduce parameter identifiability and propagate small errors across all compounds due to the summation constraint. While the performance of PLS can be enhanced by including higher-order mixtures in the training set, this approach requires substantially more calibration effort to reach a level comparable to CLS, which limits its practical applicability. Overall, the CLS model exhibits superior robustness and interpretability, particularly when analyzing complex multi-compound mixtures.

View Article Online
DOI: 10.1039/D6AY00600K

Repeatability and reproducibility were evaluated on more than 50 different samples. Repeatability, determined from consecutive measurements of the same sample under identical conditions, resulted in an average deviation of approximately 0.0005 mol mol^{-1}. Reproducibility of the Raman measurements, assessed by analyzing the same samples on different days with independent sample positioning, showed an average deviation of approximately 0.002 mol mol^{-1}. The model-related prediction accuracy obtained for binary mixtures using the CLS model (0.006 mol mol^{-1}) therefore lies within the same order of magnitude as the instrumental and measurement-related reproducibility, suggesting that the achievable quantification accuracy of the model approaches the limit imposed by experimental variability. A formal limit of detection (LOD) for each compound was not determined, as it strongly depends on the sample matrix; for example, DMC diluted in DEC differs in its detectability from DMC diluted in PC. In any case, the practical limit is governed by the parameter identifiability of the model. Raman signals observed below the lower threshold w_i^{lb} of a compound were considered indistinguishable/undetectable and are marked as n.d. in the following tables.

Composition analysis of real samples from battery recycling

Analysis of low-fluorescence mixtures (Pilot shredder samples)

Compositions of real condensate samples (yellowish) obtained from pilot shredder, which exhibited lower fluorescence (Figure 2), were analyzed using conventional Raman spectroscopy (784 nm excitation wavelength) with CLS model (equation 6) and compared with results from GC-MS, which is summarized in Table 1.

View Article Online
DOI: 10.1039/D6AY00600K

Table 1: Comparison of analyzed composition of six condensate samples from pilot shredder using GC-MS and conventional Raman spectroscopy (784 nm excitation wavelength) with CLS regression model.

Sample	Method	Mole fraction						
		DMC	EMC	DEC	EC	PC	TBB	TPB
1	GC-MS	0.50	0.45	0.02	0.03	n.d.	n.d.	n.d.
	Raman (CLS)	0.52	0.43	0.03	0.02	n.d.	n.d.	n.a.
2	GC-MS	0.22	0.67	0.05	0.06	n.d.	n.d.	n.d.
	Raman (CLS)	0.20	0.70	0.05	0.04	n.d.	n.d.	n.a.
3	GC-MS	0.08	0.70	0.04	0.10	0.05	0.03	n.d.
	Raman (CLS)	0.09	0.69	0.04	0.09	0.06	0.03	n.a.
4	GC-MS	0.05	0.83	0.03	0.06	n.d.	0.03	< 0.01
	Raman (CLS)	0.07	0.80	0.03	0.06	0.01	0.03	n.a.
5	GC-MS	0.28	0.57	0.03	0.09	n.d.	0.03	< 0.01
	Raman (CLS)	0.28	0.60	0.03	0.06	n.d.	0.03	n.a.
6	GC-MS	0.37	0.53	0.02	0.06	n.d.	0.02	< 0.01
	Raman (CLS)	0.38	0.54	0.02	0.04	n.d.	0.02	n.a.

n.d. - not detected, n.a. - not analyzed

Based on the results, conventional Raman spectroscopy is suitable for mixture analysis of real samples from battery shredding processes, exhibiting a relatively low fluorescence background. With respect to the non-fluorescing synthetic electrolyte samples, deviations in composition quantification are slightly larger but remain within acceptable limits (< 0.03 mol mol^{-1}) for rapid detection and decision-making. It should be noted that the reference GC-MS data are also subject to variability introduced during sample preparation, including dilution and handling steps, as well as minor deviations that may arise from incomplete chromatographic separation. Considering these sources of error, conventional Raman spectroscopy with a 784 nm excitation wavelength provides

View Article Online
DOI: 10.1039/D6AY00600K

sufficient accuracy for rapid online analysis of electrolyte solvent mixtures in prospective downstream processing. In the GC-MS analysis, 1-isopropoxy-2-propanol (CAS 3944-36-3) and ethyl methyl ether (CAS 540-67-0) were observed; however, the qualifier score was only 35–40%%, indicating an uncertain compound identification. Nevertheless, their presence demonstrates that real condensate samples contain some impurities, although the chromatogram qualitatively indicates only minor proportions. This also highlights a key advantage of the CLS approach: the residual spectrum allows unconsidered compounds to be detected. For example, the TPB Raman spectrum was consistently included in the fit, although it was not calibrated. Similarly, a library of pure reference substances could be incorporated and expanded as needed for future analyses. Compounds with significant weights would clearly indicate the need for calibration and inclusion in the model, analogous to the use of substance databases and qualifier scores in GC analyses.

Analysis of high-fluorescence mixtures (industrial shredder)

Regarding the spectra in Figure 2, for the strongly fluorescing condensate samples obtained from industrial shredder, conventional Raman spectroscopy with 784 nm excitation combined with tested basic mathematical processing (including polynomial and spline-based baseline subtraction, ALS baseline fitting, and wavelet transform-based filtering) was no longer sufficient to reliably extract the Raman signal from the background. In addition, a U-Net-based deep learning model[17] previously developed in our group was evaluated for fluorescence suppression but did not yield robust (with respect to quantitative composition analysis) recovery of the Raman spectral features for the investigated samples. Therefore, based on computational spectral processing, refined

View Article Online
DOI: 10.1039/D6AY00600K

spectra that enable reliable compositional analysis were not achievable. We thus took advantage of the SERDS variant of Raman spectroscopy, which on the costs of a slightly more complex Raman device and evaluation routine enables the experimental suppression of the fluorescence interference. The SERDS workflow for background suppression is shown in Figure 9.

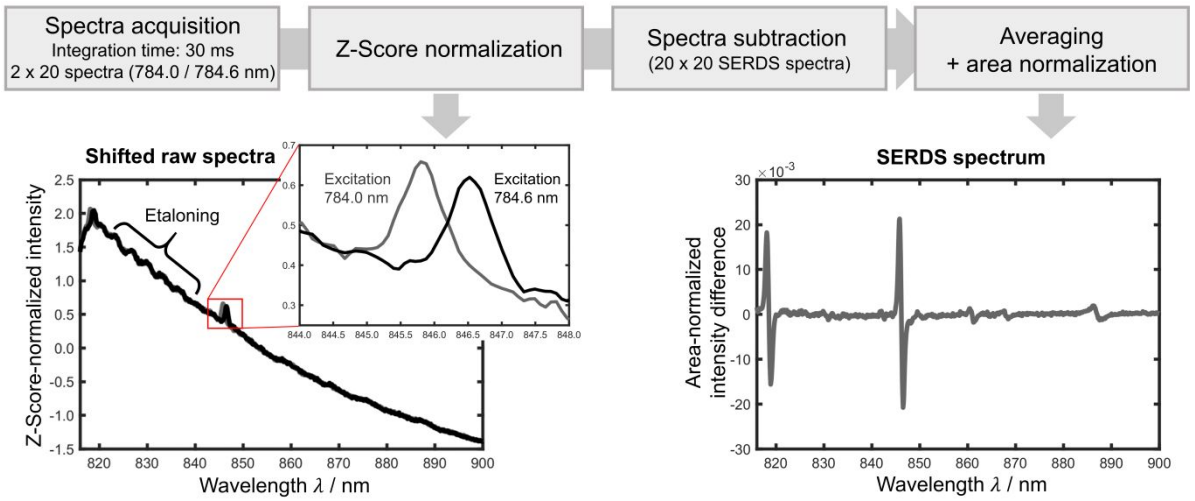

Figure 9: Spectral processing workflow to obtain the SERDS spectrum from example condensate sample from industrial shredder excited with 784.0 and 784.6 nm.

In each measurement, still 20 spectra were recorded but with reduced integration time of 30 ms. Longer integration times caused saturation of the detector due to strong fluorescence interferences. The sample remained in position while the excitation wavelength was shifted by 0.6 nm using the motorized wavelength control, after which a second set of 20 spectra was recorded. This wavelength shift of 0.6 nm (see the highlighted peak in the left diagram of Figure 9) was set based on the full width at half maximum (FWHM) of the peaks of interest to be resolved, as described by Yang et al.[39]. Therefore, the selected wavelength shift is within the spectral resolution of the

View Article Online
DOI: 10.1039/D6AY00600K

spectrometer, ensuring reliable differentiation of the shifted Raman features during SERDS processing, while at the same time the shift is sufficiently small to avoid excessive peak distortion. Spectra processing is exclusively performed in the wavelength regime, thereby avoiding distortions introduced by the nonlinear wavelength-to-Raman-shift conversion and ensuring that the spectrometer resolution is consistently applied in the native measurement domain. All spectra were z-score normalized (Figure 9 left diagram), which results in cleaner SERDS spectra compared to other normalization methods, as demonstrated by Gebrekidan et al.[22]. The SERDS spectra were explicitly calculated first, yielding 20 x 20 combinations, and then averaged. This procedure minimizes noise without additional measurements, in contrast to previously averaging (2 x 20 spectra) with subsequent subtraction. Finally, the resulting SERDS spectra were area-normalized over the absolute value of the signal for subsequent composition evaluation (Figure 9 right diagram).

Figure 9 indicates that SERDS enables extraction of a distinct Raman signal from strongly fluorescence-dominated raw spectra, with minimal remaining background, as evidenced by the SERDS spectrum being centered near the zero line with only minor fluctuations. In particular, etaloning artifacts are efficiently suppressed. Owing to the reduced integration time, however, the signal-to-noise ratio is slightly decreased relative to the conventional Raman method.

The quantitative analysis is illustrated in Figure 10 and was performed analogously to the procedure used for conventional Raman spectroscopy, but directly on SERDS spectra. SERDS spectra are in the following denoted as S'; nevertheless, the general composition evaluation strategy remains the

View Article Online
DOI: 10.1039/D6AY00600K

same. SERDS spectra of the pure substances were first determined following the workflow described above. Subsequently, the compound weights w_i were determined by fitting the pure compound SERDS spectra (Figure 10 right) directly to each measured SERDS spectrum (Figure 10 top left) through minimization of the residuals (Figure 10 bottom left gray), indicating no remaining spectral structure. Correspondingly, a new calibration (Figure 11) was established based on synthetic binary mixtures in the same manner but using SERDS spectra. In the condensate samples obtained from industrial shredder, neither TBB nor TPB were detected in GC-MS analysis. Therefore, the SERDS spectra of TBB and TPB were included in the fitting procedure but were not specifically calibrated.

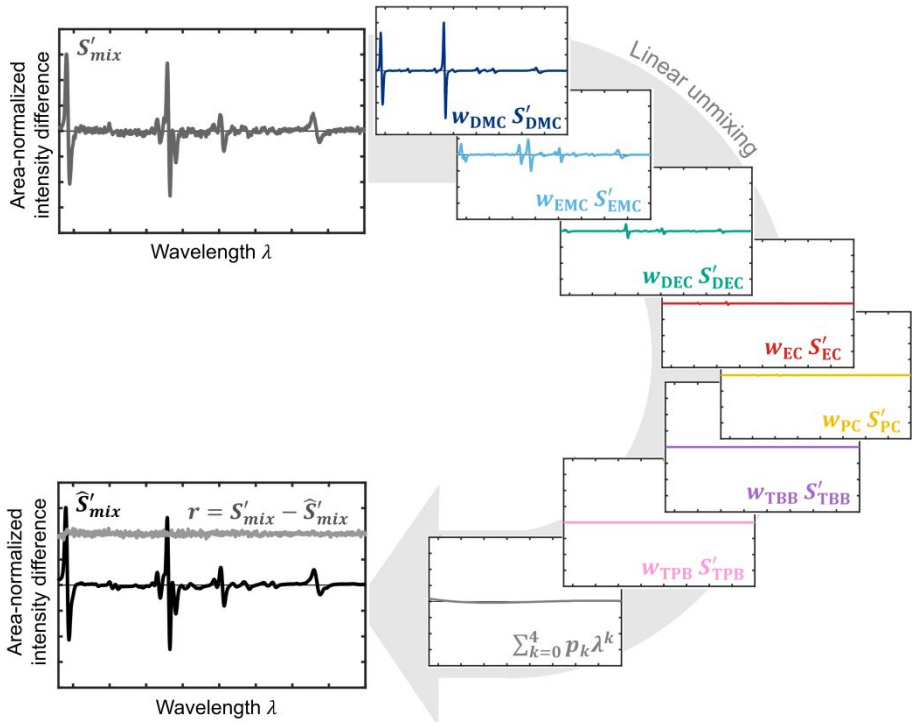

Figure 10: Linear unmixing (CLS model) of an example quinary synthetic mixture using SERDS.

View Article Online
DOI: 10.1039/D6AY00600K

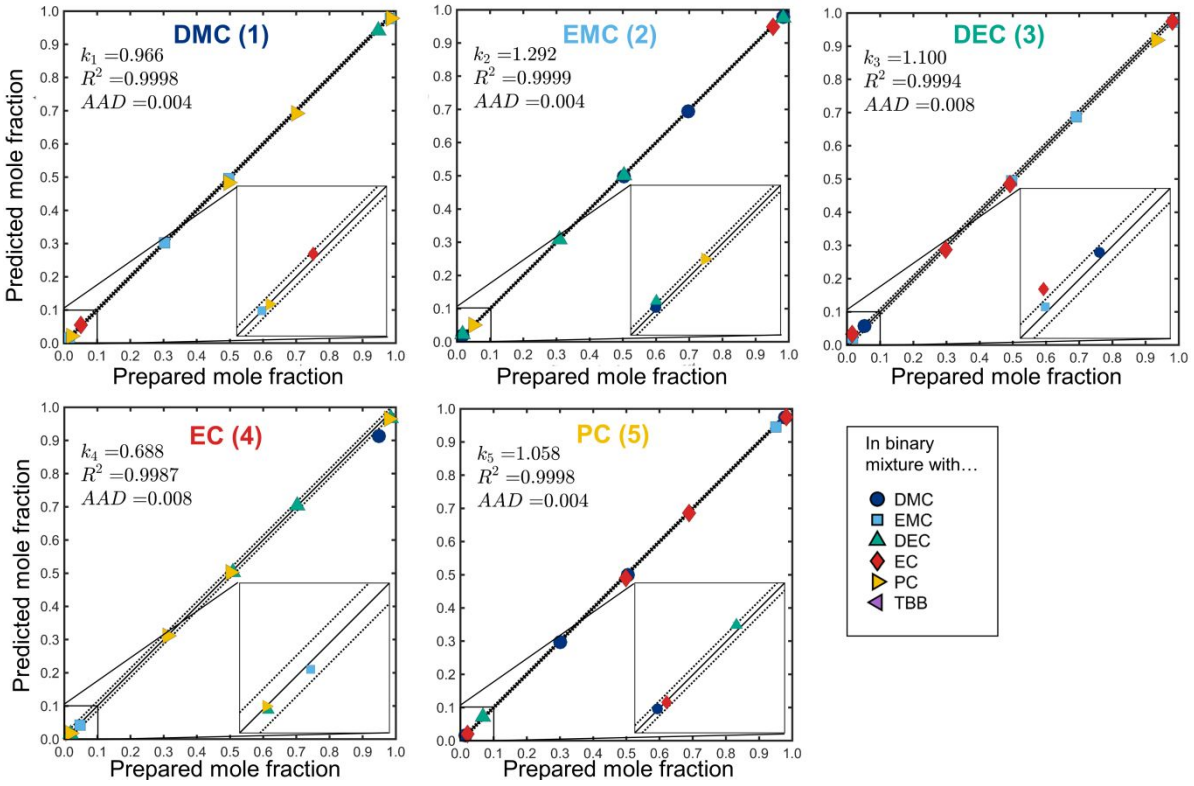

Figure 11: Fitting of calibration constants in CLS model using SERDS: Parity plots comparing predicted vs. prepared mole fraction for each compound in binary mixtures. Dotted lines represent the RMSE interval around the parity line. Error bars are not visible because the uncertainties from Raman measurement reproducibility and mixture preparation are smaller than the marker size.

Since all calibration constants are related to each other as quotients of one another through equation 5, and since the linear CLS model applies for all compound interactions (cf. Figure 6), the required calibration effort can be substantially reduced – as it was also shown for TBB in conventional Raman measurements. In contrast, this would not be feasible using PLS, highlighting the advantage of the CLS approach for handling limited calibration data. Remarkably, the mean absolute deviation for synthetic binary mixtures remains approximately 0.006 mol mol^{-1}, even though two

View Article Online
DOI: 10.1039/D6AY00600K

spectra per sample were time-delayed recorded and additional data processing steps were required, demonstrating both the repeatability of the measurements and the robustness of the model.

Analogously, compositions of colored condensate samples from industrial shredder were quantified using SERDS evaluated with the CLS model, and GC-MS analysis serving as reference. Since the original samples had similar compositions, more high-fluorescence samples were synthesized by spiking sample 3 with defined amounts of additional pure electrolyte solvent compounds. The results are reported in Table 2.

Table 2: Comparison of analyzed composition of five condensate samples from industrial shredder using GC-MS and SERDS with CLS regression model. Mixtures 3-1 to 3-4 are synthesized by spiking (weighing) sample 3 with pure compounds using analyzed composition from GC-MS.

Sample	Method	Mole fraction				
		DMC	EMC	DEC	EC	PC
1	GC-MS	0.78	0.19	0.01	0.01	n.d.
	SERDS	0.80	0.18	< 0.01	0.02	n.d.
2	GC-MS	0.82	0.16	< 0.01	0.02	n.d.
	SERDS	0.84	0.13	0.02	0.02	n.d.
3	GC-MS	0.81	0.17	< 0.01	0.02	n.d.
	SERDS	0.84	0.15	< 0.01	0.01	n.d.
4	GC-MS	0.83	0.16	< 0.01	0.02	n.d.
	SERDS	0.86	0.12	0.01	0.01	n.d.
5	GC-MS	0.81	0.16	< 0.01	0.02	n.d.
	SERDS	0.84	0.13	0.02	0.01	n.d.
3-1	GC-MS (synth.)	0.46	0.09	0.44	0.01	n.d.
	SERDS	0.47	0.06	0.45	0.01	0.01

View Article Online
DOI: 10.1039/D6AY00600K

3-2	GC-MS (synth.)	0.44	0.44	0.11	0.01	n.d.
	SERDS	0.44	0.43	0.11	0.01	0.01
3-3	GC-MS (synth.)	0.56	0.11	0.10	0.12	0.11
	SERDS	0.58	0.10	0.10	0.11	0.11
3-4	GC-MS (synth.)	0.69	0.14	0.06	0.05	0.06
	SERDS	0.73	0.10	0.06	0.05	0.06

n.d. - not detected, n.a. - not analyzed

Considering the strongly overlapping background in the raw spectra, the compositions can still be determined with high accuracy, although deviations increase compared to the less fluorescent samples from the pilot shredder. Here, a systematic shift is observed between DMC and EMC, which is reduced in the spiked samples. The dilution of the fluorescent samples has only minor effect on the curvature of the fluorescence background, but decreases its relative contribution to the overall signal intensity. Therefore, the signal-to-noise ratio of the processed SERDS spectra of the spiked samples is improved compared to that of the original condensate samples from LIB shredder. This suggests that the lower signal-to-noise ratio of spectra from fluorescence-dominated mixtures may impair the reliable assignment of spectral features and could therefore contribute to such systematic shifts observed. However, it could not be finally determined whether the deviations arise from a combination of different factors, including spectral overlap, calibration limitations, or sample matrix effects in both, Raman or GC-MS analysis. While the calibration effort can be substantially reduced due to the relationships between the constants k_i/k_j (equation 4), slight deviations may occur when applied to real samples. Nevertheless, the results demonstrate that SERDS enables efficient fluorescence suppression, while preserving the main Raman spectral features for robust and reliable composition analysis in combination with the CLS model. This

View Article Online
DOI: 10.1039/D6AY00600K

highlights its suitability for prospective in-line measurements in battery recycling applications with complex spectral interferences. Based on this, future work will focus on further refinement of this method based on a more comprehensive set of real condensate samples from industrial LIB recycling. Additional compounds revealed by GC-MS, including propane, 2,2-dimethoxy (CAS: 77-76-9), 1,3-dioxolane (CAS: 2916-31-6), 4-methyl-3-penten-2-one (CAS: 141-79-7), and 4-Hydroxy-4-methyl-2-pentanone (CAS: 123-42-2) are likely minor decomposition or side products originating from some degradation of the main organic carbonates. Their molecular structures indicate plausible formation pathways from DMC, EMC, DEC, EC, and PC, for example via hydrolysis, cyclization, or elimination reactions. Due to their low abundance in the chromatogram and the unstructured residuals in SERDS evaluation, these compounds are not considered in the composition analysis presented here – intended to support rapid decision-making, such as preliminary sorting or other downstream processes in battery recycling.

Conclusions

In this work, Raman spectroscopy combined with CLS regression was demonstrated as a robust and efficient method for the quantitative analysis of electrolyte solvent mixtures from LIB recycling, requiring less calibration effort than PLS regression. In addition, CLS enables straightforward extension of the model by incorporating spectra of minor species, while still providing quantitative results even if these species are not explicitly calibrated.

The application to real condensate samples confirmed the robustness of the method, even under challenging conditions. The use of shifted excitation Raman difference spectroscopy (SERDS)

View Article Online
DOI: 10.1039/D6AY00600K

enabled reliable extraction of Raman signals and efficient suppression of fluorescence and etaloning. With a total spectra acquisition time of 1.2 s (40 x 30 ms), approximately 1 s for motorized wavelength shifting, and 2 s for computation, the method is well suited for rapid analysis, offering further potential for optimization with application-tailored instrumentation.

In particular, Raman spectroscopy is characterized by straightforward data evaluation, simple and robust calibration procedure, and flexible integration into existing process environments. In order to enable real-time process control and fast decision-making in battery recycling operations, future work should investigate the integration of the method into real in-line monitoring systems, while maintaining process safety and compliance with operational constraints such as explosion protection.

Author contributions

Tom Goldberg: writing – original draft, methodology, investigation, formal analysis, visualization.

Roland Haseneder: writing – review & editing, investigation (GC-MS analysis).

Andreas S. Braeuer: writing – review & editing, conceptualization, methodology, supervision.

Conflicts of interest

There are no conflicts to declare.

Data availability

View Article Online
DOI: 10.1039/D6AY00600K

This study was not part of a funded project. The recorded spectra have potential commercial value and are therefore not publicly available. All data supporting the findings of this study are included in tabular form within this article. The MATLAB codes used can be made available upon request.

Acknowledgements

The authors acknowledge the Institute of Mechanical Process Engineering and Mineral Processing at TU Bergakademie Freiberg as well as BASF SE for providing the real electrolyte samples from their LIB shredder.

View Article Online
DOI: 10.1039/D6AY00600K

References

1 *Regulation (EU) 2023/1542 of the European Parliament and of the Council of 12 July 2023 concerning batteries and waste batteries, amending Directive 2008/98/EC and Regulation (EU) 2019/1020 and repealing Directive 2006/66/EC, Annex XII, Part B*, 2023.

2 Z. Lu, L. Ning, X. Zhu and H. Yu, Critical Pathways for Transforming the Energy Future: A Review of Innovations and Challenges in Spent Lithium Battery Recycling Technologies, *Materials (Basel, Switzerland)*, 2025, **18**. DOI: 10.3390/ma18132987.

3 F. Arshad, L. Li, K. Amin, E. Fan, N. Manurkar, A. Ahmad, J. Yang, F. Wu and R. Chen, A Comprehensive Review of the Advancement in Recycling the Anode and Electrolyte from Spent Lithium Ion Batteries, *ACS Sustainable Chem. Eng.*, 2020, **8**, 13527–13554.

4 J. Fang, G. Wan, M. Zheng, T. Liu and J. Lu, Recycling of Spent Lithium-Ion Batteries in View of Lithium, *Advanced Energy Materials*, 2025, **15**. DOI: 10.1002/aenm.202501318.

5 T. Georgi-Maschler, B. Friedrich, R. Weyhe, H. Heegn and M. Rutz, Development of a recycling process for Li-ion batteries, *Journal of Power Sources*, 2012, **207**, 173–182.

6 E. Smith and G. Dent, *Modern Raman Spectroscopy – A Practical Approach*, Wiley, 2004.

7 R. W. Kessler, ed., *Prozessanalytik. Strategien und Fallbeispiele aus der industriellen Praxis*, Wiley-VCH, Weinheim, 2006.

View Article Online
DOI: 10.1039/D6AY00600K

8 S. Paprocki, M. Qassem and P. A. Kyriacou, The Impact of Acetic Acid on Measuring Ethanol Concentrations in Water and Human Serum Using Short-Wave Infrared Spectroscopy, *International journal of molecular sciences*, 2023, **24**. DOI: 10.3390/ijms24032980.

9 A. Rogalski, P. Martyniuk, M. Kopytko and W. Hu, Trends in Performance Limits of the HOT Infrared Photodetectors, *Applied Sciences*, 2021, **11**, 501.

10 S. Kainat, J. Anwer, A. Hamid, N. Gull and S. M. Khan, Electrolytes in Lithium-Ion Batteries: Advancements in the Era of Twenties (2020's), *Materials Chemistry and Physics*, 2024, **313**, 128796.

11 R. Zhang, X. Shi, O. C. Esan and L. An, Organic Electrolytes Recycling From Spent Lithium-Ion Batteries, *Global challenges (Hoboken, NJ)*, 2022, **6**, 2200050.

12 C. Hartnig and M. Schmidt, in *Lithium-Ion Batteries: Basics and Applications*, ed. R. Korthauer, Springer Berlin Heidelberg, Berlin, Heidelberg, 2018, pp. 59–74.

13 M. Ue, Y. Sasaki, Y. Tanaka and M. Morita, in *Electrolytes for Lithium and Lithium-Ion Batteries*, ed. T. R. Jow, K. Xu, O. Borodin and M. Ue, Springer New York, New York, NY, 2014, pp. 93–165.

14 M. Wolke, K. Schröder, K. Arnold, P. Mozumder, T. Beuerle, K. Jasch and S. Scholl, Analyzing Organic Electrolyte Solvents from Spent Lithium-Ion Batteries as a Basis for Distillative Value Component Recovery, *Recycling*, 2025, **10**, 19.

15 D. Wei, S. Chen and Q. Liu, Review of Fluorescence Suppression Techniques in Raman Spectroscopy, *Applied Spectroscopy Reviews*, 2015, **50**, 387–406.

View Article Online
DOI: 10.1039/D6AY00600K

16 A. G. Ryder, G. M. O'Connor and T. J. Glynn, Identifications and Quantitative Measurements of Narcotics in Solid Mixtures Using Near-IR Raman Spectroscopy and Multivariate Analysis, *Journal of Forensic Sciences*, 1999, **44**, 1013–1019.

17 F. C. Thorley, K. J. Baldwin, D. C. Lee and D. N. Batchelder, Dependence of the Raman spectra of drug substances upon laser excitation wavelength, *J Raman Spectroscopy*, 2006, **37**, 335–341.

18 M. Kasha, Characterization of electronic transitions in complex molecules, *Discuss. Faraday Soc.*, 1950, **9**, 14.

19 G. Schulze, A. Jirasek, M. M. L. Yu, A. Lim, R. F. B. Turner and M. W. Blades, Investigation of selected baseline removal techniques as candidates for automated implementation, *Applied spectroscopy*, 2005, **59**, 545–574.

20 J. J. Schuster, L. A. Bahr, L. Fehr, M. Tippelt, J. Schulmeyr, A. Wuzik and A. S. Braeuer, Online monitoring of the supercritical CO2 extraction of hop, *The Journal of Supercritical Fluids*, 2018, **133**, 139–145.

21 M. T. Gebrekidan, C. Knipfer, F. Stelzle, J. Popp, S. Will and A. Braeuer, A shifted-excitation Raman difference spectroscopy (SERDS) evaluation strategy for the efficient isolation of Raman spectra from extreme fluorescence interference, *J Raman Spectroscopy*, 2016, **47**, 198–209.

View Article Online
DOI: 10.1039/D6AY00600K

22 H. Sheridan, A. P. Dudgeon, J. C. C. Day, C. Kendall, C. Hall and N. Stone, Optimising Shifted Excitation Raman Difference Spectroscopy (SERDS) for application in highly fluorescent biological samples, using fibre optic probes, *The Analyst*, 2024, **150**, 103–119.

23 J. Y. Qu, B. C. Wilson and D. Suria, Concentration measurements of multiple analytes in human sera by near-infrared laser Raman spectroscopy, *Applied optics*, 1999, **38**, 5491–5498.

24 E. Kriesten, D. Mayer, F. Alsmeyer, C. B. Minnich, L. Greiner and W. Marquardt, Identification of unknown pure component spectra by indirect hard modeling, *Chemometrics and Intelligent Laboratory Systems*, 2008, **93**, 108–119.

25 S. K. Luther, J. J. Schuster, A. Leipertz and A. Braeuer, Non-invasive quantification of phase equilibria of ternary mixtures composed of carbon dioxide, organic solvent and water, *The Journal of Supercritical Fluids*, 2013, **84**, 146–154.

26 R. Adami, J. Schuster, S. Liparoti, E. Reverchon, A. Leipertz and A. Braeuer, A Raman spectroscopic method for the determination of high pressure vapour liquid equilibria, *Fluid Phase Equilibria*, 2013, **360**, 265–273.

27 Y. Chen and L. Dai, A Method for the Quantitative Analysis of a Key Component in Complex Mixtures Using Raman Spectroscopy Based on Peak Decomposition, *Analytical sciences : the international journal of the Japan Society for Analytical Chemistry*, 2019, **35**, 511–515.

28 A. Weber-Bernard and J. Viell, Raman spectroscopy for determination of compositions in liquid–liquid dispersions, *Results in Chemistry*, 2025, **16**, 102419.

View Article Online
DOI: 10.1039/D6AY00600K

29 B. Liebergesell, T. Brands, H.-J. Koß and A. Bardow, Quaternary isothermal vapor-liquid equilibrium of the model biofuel 2-butanone + n-heptane + tetrahydrofuran + cyclohexane using Raman spectroscopic characterization, *Fluid Phase Equilibria*, 2018, **472**, 107–116.

30 A. M. K. Enejder, T.-W. Koo, J. Oh, M. Hunter, S. Sasic, M. S. Feld and G. L. Horowitz, Blood analysis by Raman spectroscopy, *Optics letters*, 2002, **27**, 2004–2006.

31 E. Kriesten, F. Alsmeyer, A. Bardow and W. Marquardt, Fully automated indirect hard modeling of mixture spectra, *Chemometrics and Intelligent Laboratory Systems*, 2008, **91**, 181–193.

32 S. Wold, M. Sjöström and L. Eriksson, PLS-regression: a basic tool of chemometrics, *Chemometrics and Intelligent Laboratory Systems*, 2001, **58**, 109–130.

33 F. Alsmeyer, H.-J. Koss and W. Marquardt, Indirect spectral hard modeling for the analysis of reactive and interacting mixtures, *Applied spectroscopy*, 2004, **58**, 975–985.

34 M. Willger and A. S. Braeuer, Thermodynamically consistent derivation of excess Raman spectra, *J Raman Spectroscopy*, 2024, **55**, 1080–1089.

35 F. Gan, G. Ruan and J. Mo, Baseline correction by improved iterative polynomial fitting with automatic threshold, *Chemometrics and Intelligent Laboratory Systems*, 2006, **82**, 59–65.

36 P. H. C. Eilers and H. F. M. Boelens, *Baseline correction with asymmetric least squares smoothing*, Leiden University Medical Centre, Leiden, 2005.

37 A. Bräuer, *In situ spectroscopic techniques at high pressure*, Elsevier, Amsterdam, Boston, Heidelberg, Oxford, 2015.

View Article Online
DOI: 10.1039/D6AY00600K

38 S. Yang, B. Li, M. N. Slipchenko, A. Akkus, N. G. Singer, Y. N. Yeni and O. Akkus, Laser Wavelength Dependence of Background Fluorescence in Raman Spectroscopic Analysis of Synovial Fluid from Symptomatic Joints, *J Raman Spectroscopy*, 2013, **44**, 1089–1095.

View Article Online
DOI: 10.1039/D6AY00600K

Data availability

This study was not part of a funded project. The recorded spectra have potential commercial value and are therefore not publicly available. All data supporting the findings of this study are included in tabular form within this article. The MATLAB codes used can be made available upon request.